Improving the Efficiency of Computing Electromagnetic Fields from a Lossy Dielectric Cylinder due to a Line Source

Grant A. Ellis

Department of Electrical and Electronic Engineering
Nazarbayev University, Astana 010000, Kazakhstan
grant.ellis@gmail.com

Abstract ─ This paper describes analysis of electromagnetic fields from a lossy dielectric cylinder due to a line source. Series solutions for the electromagnetic fields internal and external to the cylinder are derived. Convergence is accelerated using the Watson transformation and the "*fast_callable*" function in the SageMath™ open source software. The series convergence is increased by a factor of nearly 80 using these techniques. Implementation of the Watson transform is also discussed. Applications include propagation analysis for simulating wireless body area networks and communications with wireless biosensors.

Index Terms ─ Bioelectromagnetics, creeping waves, SageMath™, Watson transform, WBAN.

I. INTRODUCTION

Wireless body area networks (WBAN) are increasingly being considered for use in wireless computing. Initially, WBAN research was for use at Wi-Fi frequencies and has been extended to UWB and is currently being studied for use in the 57-65 GHz license free band [1-4]. On-body communications can be used for medical diagnostics and monitoring patients in real-time. Applications include communications with wireless implants or bio-sensors mounted on skin or deposited inside tissue, e.g., communications with a field probe located inside a dressing [5]. Full-wave electromagnetic analysis of the human torso above 10 GHz becomes prohibitive in terms of memory.

SageMath™ is an open-source Python-based mathematics software system licensed under GPL. It is a high-level interpreted programming language for interactive use with access to several open-source packages including NumPy, SciPy, Maxima, SumPy, R, and Matplotlib [6]. It can also evaluate both symbolic and Python-type functions. It is an especially well-suited computing environment for solving analytical electromagnetics problems.

This paper is organized as follows; in Section II, analytical expressions are derived for determining the electromagnetic fields due to a line source in the presence of a lossy dielectric cylinder for TE and TM polarizations. These fields are considered for locations that are internal and external of the cylinder. In Section III, Watson series solutions are introduced to accelerate convergence. In Section IV, validation with a numerical approach is given. In Section V, results for attenuation of the fields from a dielectric cylinder used to model a human torso are given. In Section VI, computational issues such as convergence, timing, and programming are discussed. Finally, the paper is concluded.

II. THEORETICAL DEVELOPMENT

The complex dielectric properties of wet and dry skin tissue are well-known [7]. Skin conductivity (σ) increases monotonically while the relative permittivity (ε_r) decreases monotonically with increasing frequency. As a result, the penetration depth decreases with increasing frequency and is only about 2.2 cm at 2.5 GHz for dry skin. In this paper, an electric or magnetic line source located near a lossy dielectric cylinder is used to simulate the source near a human body. The configuration used for the simulations is shown in Fig. 1. The dielectric cylinder is assumed to be two-dimensional ($\partial/\partial z = 0$) with radius a, and constitutive parameters μ_r, σ, and ε_r. Cylindrical coordinates are used for the source (ρ', ϕ') and observer (ρ, ϕ) locations. The $e^{-i\omega t}$ time variation is also assumed. The line source is assumed to be external to the cylinder.

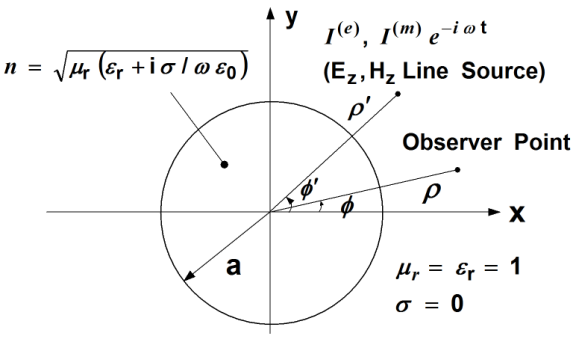

Fig. 1. Diagram of dielectric cylinder and line source.

Submitted On: October 10, 2016
Accepted On: June 14, 2017

The axial components $\Pi_z^{(e)}$ and $\Pi_z^{(m)}$ of the Hertzian vectors must satisfy [8]:

$$\left(\frac{1}{\rho}\frac{\partial}{\partial\rho}\rho\frac{\partial}{\partial\rho}+\frac{1}{\rho^2}\frac{\partial^2}{\partial\varphi^2}+k_0^2\right)\Pi_z^{(e)} = \begin{cases} -\dfrac{i\,I^{(e)}}{\omega\,\varepsilon_0}\dfrac{\delta(\rho-\rho')\,\delta(\phi-\phi')}{\rho}, & \rho > a \\ 0, & \rho < a \end{cases}, \quad (1a)$$

and

$$\left(\frac{1}{\rho}\frac{\partial}{\partial\rho}\rho\frac{\partial}{\partial\rho}+\frac{1}{\rho^2}\frac{\partial^2}{\partial\varphi^2}+k_0^2\right)\Pi_z^{(m)} = \begin{cases} -\dfrac{i\,I^{(m)}}{\omega\,\mu_0}\dfrac{\delta(\rho-\rho')\,\delta(\phi-\phi')}{\rho}, & \rho > a \\ 0, & \rho < a \end{cases}. \quad (1b)$$

Solutions for $\Pi_z^{(e)}$ and $\Pi_z^{(m)}$ are both of the form:

(i) Outside the cylinder, ρ > ρ',

$$\Pi = A(\rho')\sum_{-\infty}^{\infty}\frac{i\,I}{2\,\pi\,\omega}\,exp\,\left[im(\phi-\phi')\right]H_m^{(1)}(k_0\,\rho). \quad (2a)$$

(ii) Between the cylinder and source, a < ρ < ρ',

$$\Pi = \sum_{-\infty}^{\infty}\frac{i\,I}{2\pi\omega}\,exp[im(\phi-\phi')]\times \left\{B(\rho')J_m(k_0\rho)+C(\rho')H_m^{(1)}(k_0\rho)\right\}. \quad (2b)$$

(iii) Inside the cylinder, ρ < a,

$$\Pi = D(\rho')\sum_{-\infty}^{\infty}\frac{i\,I\,n^2}{2\,\pi\,\omega}\,exp\,\left[im(\phi-\phi')\right]J_m(k\rho). \quad (2c)$$

The coefficients *A*-*D* are uniquely determined by enforcing the tangential boundary conditions for continuity of E_z and H_ϕ for the TE case (electric field perpendicular to x-y plane) and E_ϕ and H_z for the TM case (magnetic field perpendicular to x-y plane) at ρ = a. In addition, the solutions for Π above in (2a) and (2b) must be continuous due to the line source at ρ = ρ'.

After solving for these Hertz potentials, the individual *E*- and *H*-field components can then be found. For example, the axial field components outside the cylinder ρ > a are:

$$E_z = k_0^2\,\Pi_z^{(e)} \text{ and } H_z = k_0^2\,\Pi_z^{(m)}, \quad (3a)$$

and interior of the cylinder ρ < a as:

$$E_z = k_0^2\,n^2\,\Pi_z^{(e)} \text{ and } H_z = k_0^2\,n^2\Pi_z^{(m)}. \quad (3b)$$

The resulting total fields inside and outside the cylinder are [8]:

A. Fields outside of cylinder for TE or E_z polarization,

$$E_z = -I^{(e)}\frac{k_0^2}{4\,\omega\varepsilon_0}\sum_{-\infty}^{\infty}\exp\left[im(\varphi-\varphi')\right]H_m^{(1)}(k_0\rho) \times\left[J_m(k_0\rho')-\frac{J_m(k_0a)-Z^{(e)}J_m'(k_0a)}{H_m^{(1)}(k_0a)-Z^{(e)}H_m'^{(1)}(k_0a)}H_m^{(1)}(k_0\rho')\right], \quad (4a)$$

where ρ > ρ' and $Z^{(e)} = \dfrac{\mu_r\,J_m(ka)}{n\,J_m'(ka)}$.

B. Fields outside of cylinder for TM or H_z polarization,

$$H_z = -I^{(m)}\frac{k_0^2}{4\,\omega\mu_0}\sum_{-\infty}^{\infty}\exp\left[im(\varphi-\varphi')\right]H_m^{(1)}(k_0\rho) \times\left[J_m(k_0\rho')-\frac{J_m'(k_0a)-Z^{(m)}J_m(k_0a)}{H_m'^{(1)}(k_0a)-Z^{(m)}H_m^{(1)}(k_0a)}H_m^{(1)}(k_0\rho')\right], \quad (4b)$$

where ρ > ρ' and $Z^{(m)} = \dfrac{\mu_r\,J_m'(ka)}{n\,J_m(ka)}$.

The source (ρ', ϕ') and observer (ρ, ϕ) locations can be interchanged by simply interchanging the primed and unprimed coordinates. The internal fields are:

C. Fields inside of cylinder (ρ < a) for TE or Ez polarization,

$$E_z = -I^{(e)}\frac{k_0^2}{4\,\omega\varepsilon_0}\sum_{-\infty}^{\infty}\exp\left[im(\varphi-\varphi')\right]H_m^{(1)}(k_0\rho')\,J_m(k\rho) \times\left[\frac{J_m(k_0a)+R^{(e)}(m)H_m^{(1)}(k_0a)}{J_m(k\,a)}\right], \quad (5a)$$

where $R^{(e)}(m) = -\left[\dfrac{J_m(k_0a)-Z^{(e)}J_m'(k_0a)}{H_m^{(1)}(k_0a)-Z^{(e)}H_m'^{(1)}(k_0a)}\right]$.

D. Fields inside of cylinder (ρ < a) for Hz or TM polarization,

$$H_z = -I^{(m)}\frac{k_0^2}{4\,\omega\mu_0}\sum_{-\infty}^{\infty}\exp\left[im(\varphi-\varphi')\right]H_m^{(1)}(k_0\rho')\,J_m(k\rho) \times\left[\frac{J_m(k_0a)+R^{(m)}(m)H_m^{(1)}(k_0a)}{J_m(k\,a)}\right], \quad (5b)$$

where $R^{(m)}(m) = -\left[\dfrac{J_m'(k_0a)-Z^{(m)}J_m(k_0a)}{H_m'^{(1)}(k_0a)-Z^{(m)}H_m^{(1)}(k_0a)}\right]$.

III. CONVERGENCE ACCELERATION

It is well-known that the series solutions like those shown in (4a) and (4b) converge very slowly when k_0a is large. As a consequence, many terms are required to obtain reasonable accuracy. A technique known as Watson's Theorem or sometimes as Poisson's Summation

Formula can be used to accelerate the convergence of these series [8-10]. Watson's transform essentially converts (4a) and (4b) into another series by calculating the sum of the residues at their poles.

The advantage of using the Watson Transform is that a series requiring hundreds of terms or more to converge can be replaced with another series requiring only a few terms to converge. Also, the pole locations used for determining the residues are calculated only once for a particular dielectric cylinder and frequency but can be used with any source or receiver location. The disadvantage is the additional step required to compute the pole locations for computing the residues.

Equations (4a) and (4b) can be evaluated for source $\phi' = 0$ in the complex plane by using the identity [8]:

$$\sum_{-\infty}^{\infty} \exp[im\phi]\, B_m = \frac{i}{2} \int_c \frac{\exp\left[i\nu\left(\phi - \pi\right)\right] B_\nu}{\sin(\nu\pi)}\, d\nu, \qquad (6)$$

$=-2\pi i$ times the sum of the residues of $\exp\left[i\nu(\phi-\pi)\right] B_\nu / \sin(\nu\pi)$. The singularities of B_m are simple poles of the denominator of B_m and not on the real axis. Furthermore, it can be shown that the RHS of (6) is equal to:

$$i \int_{-\infty}^{\infty} \frac{\cos\left[i\nu\left(\phi - \pi\right)\right] B_\nu}{\sin(\nu\pi)}\, d\nu.$$

The resulting E_z, H_z fields for the electric line source $I^{(e)}$ then become ($\rho > \rho'$):

$$E_z = 2\pi i \cdot I^{(e)} \frac{k_0^2}{4\,\omega\,\varepsilon_0} \cdot \sum_{j=1}^{\infty} \frac{\cos\left[\nu_j\left(\phi - \pi\right)\right]}{\sin\left(\nu_j\,\pi\right)} H_{\nu_j}^{(1)}(k_0\rho)\, H_{\nu_j}^{(1)}(k_0\rho') \times \left[\frac{J_{\nu_j}(k_0 a) - Z^{(e)} J'_{\nu_j}(k_0 a)}{\frac{\partial}{\partial \nu}\left(H_\nu^{(1)}(k_0 a) - Z^{(e)} H_\nu'^{(1)}(k_0 a)\right)\Big|_{\nu=\nu_j}} \right], \qquad (7a)$$

and for the magnetic line source $I^{(m)}$:

$$H_z = 2\pi i \cdot I^{(m)} \frac{k_0^2}{4\,\omega\,\mu_0} \cdot \sum_{j=1}^{\infty} \frac{\cos\left[\nu'_j\left(\phi - \pi\right)\right]}{\sin\left(\nu'_j\pi\right)} H_{\nu'_j}^{(1)}(k_0\rho)\, H_{\nu'_j}^{(1)}(k_0\rho') \times \left[\frac{J'_{\nu'_j}(k_0 a) - Z^{(m)} J_{\nu'_j}(k_0 a)}{\frac{\partial}{\partial \nu}\left(H_\nu'^{(1)}(k_0 a) - Z^{(m)} H_\nu^{(1)}(k_0 a)\right)\Big|_{\nu=\nu'_j}} \right], \qquad (7b)$$

where ν_j, ν_j' are the singularities of B_ν and zeroes with respect to order, ν, of:

$H_\nu^{(1)}(k_0 a) - Z^{(e)} H_\nu'^{(1)}(k_0 a) = 0$ for TE and,

$H_\nu'^{(1)}(k_0 a) - Z^{(m)} H_\nu^{(1)}(k_0 a) = 0$ for TM polarization.

$\frac{\partial H_\nu^{(1)}(k_0 a)}{\partial \nu}$ and $\frac{\partial H_\nu'^{(1)}(k_0 a)}{\partial \nu}$ are computed using SageMath™ using Python-type functions from the definitions for the derivatives of Hankel functions with respect to order provided in [11, 12]. In [12], closed-from expressions are given for the first-order derivatives of Bessel ($J\nu(\,)$) and Neumann ($Y\nu(\,)$) functions with respect to order.

A. Approximations for $Z^{(e)}$ and $Z^{(m)}$

Recall the definitions for $Z^{(e)}$ and $Z^{(m)}$ in (4a) and (4b). For large argument where $z = |k_0 na| = |k\,a| >> 1$, which is typical for WBANs at microwave frequencies the following approximations for $J_\nu(z)$ can be used:

$$J_\nu(z) \approx \sqrt{\frac{2}{\pi z}} \cos\left(z - \frac{\pi\,\nu}{2} - \frac{\pi}{4}\right), \qquad (8a)$$

and

$$\frac{\partial\, J_\nu(z)}{\partial z} \approx -\sqrt{\frac{2}{\pi z}} \sin\left(z - \frac{\pi\,\nu}{2} - \frac{\pi}{4}\right) + O\left(z^{-3/2}\right). \qquad (8b)$$

Since $|ka|$ is large (>>1) then substitution of (8a) and (8b) into the definitions for $Z^{(e)}$ and $Z^{(m)}$ yield:

$$Z^{(e)} \approx -\frac{\mu_r}{n} \frac{\cos(ka - \frac{\pi\,\nu}{2} - \frac{\pi}{4})}{\sin(ka - \frac{\pi\,\nu}{2} - \frac{\pi}{4})} = -\frac{\mu_r}{n} \cot(ka - \frac{\pi\,\nu}{2} - \frac{\pi}{4}), \qquad (8c)$$

and

$$Z^{(m)} \approx -\frac{\mu_r}{n} \frac{\sin(ka - \frac{\pi\,\nu}{2} - \frac{\pi}{4})}{\cos(ka - \frac{\pi\,\nu}{2} - \frac{\pi}{4})} = -\frac{\mu_r}{n} \tan(ka - \frac{\pi\,\nu}{2} - \frac{\pi}{4}). \qquad (8d)$$

For complex $z = x + iy$, the identity:

$$\tan(z) = \frac{\sin\,(2x) + i\,\sinh\,(2y)}{\cos\,(2x) + \cosh\,(2y)},$$

can be applied to these approximations $Z^{(e)}$ and $Z^{(m)}$. For $y >> 1$ which is the case when $k_0 a$ is large, then it can be easily seen that $\tan(z) \sim i$.

From the preceding discussion for a lossy dielectric or biological material in the cylinder if imag(ka) >>1; therefore,

$$Z^{(e)} \approx i\,\frac{\mu_r}{n} \quad \text{and} \quad Z^{(m)} \approx -i\,\frac{\mu_r}{n}. \qquad (8e)$$

These approximations for $Z^{(e)}$ and $Z^{(m)}$ in (8e) can then be used in evaluating (7a) and (7b). Next, a simple procedure for determining for the simple pole locations in (7a) and (7b) can be found.

B. Procedure for determining ν_j pole locations for TE Case and ν_j' pole locations for TM Case

Using these approximations for $Z^{(e)}$ and $Z^{(m)}$, a simple procedure for determining the simple pole

locations, ν, in (7a) and (7b) is as follows: (i) for the TE polarization,

$$H_\nu^{(1)}(k_0 a) - Z^{(e)} H_\nu'^{(1)}(k_0 a) \approx H_\nu^{(1)}(k_0 a) - \frac{i\mu_r}{n} H_\nu'^{(1)}(k_0 a) = 0 , \quad (9a)$$

and, (ii) for the TM polarization,

$$H_\nu'^{(1)}(k_0 a) - Z^{(m)} H_\nu^{(1)}(k_0 a) \approx H_\nu'^{(1)}(k_0 a) + \frac{i\mu_r}{n} H_\nu^{(1)}(k_0 a) = 0 . \quad (9b)$$

In [13], the ν_j values are approximated using:

$$\nu_j = k_0 a - e^{i\pi/3}(k_0 a/2)^{1/3}\alpha_j + \frac{i\mu_r}{n}\left(1 - \frac{e^{i\pi/3}}{15(k_0 a/2)^{2/3}}\right) - \frac{e^{-i\pi/3}}{60(k_0 a/2)^{1/3}}\alpha_j^2 , \quad (10a)$$

for the TE polarization where α_j are the zero's of the Airy function and can be approximated as [14]:

$$\alpha_j \approx -\left[\frac{3\pi}{2}\left(j - \frac{1}{4}\right)\right]^{2/3} . \quad (10b)$$

For the TM polarization, the ν_j' values are approximated also using [13]:

$$\nu_j' = k_0 a - e^{i\pi/3}(k_0 a/2)^{1/3}\alpha_j' - \frac{i\mu_r}{n} e^{-i\pi/3}(k_0 a)^{2/3}\left(\frac{1}{\alpha_j'} + \frac{e^{i\pi/3}}{15(k_0 a/2)^{2/3}}\right) - \frac{e^{-i\pi/3}}{10(k_0 a/2)^{1/3}}\left(\frac{-1}{\alpha_j'} + \frac{\alpha_j'^2}{6}\right), \quad (11a)$$

where α_j' are the zero's of the derivative of the Airy function and can be approximated as [14]:

$$\alpha_j' \approx -\left[\frac{3\pi}{2}\left(j - \frac{3}{4}\right)\right]^{2/3} . \quad (11b)$$

The approximations in (8e) are used to approximate the solutions to (9a) and (9b) above and result in the approximate solutions for ν_j and ν_j' shown in (10a) and (11a). The exact values for ν_j and ν_j' can be determined using an iterative method such as Newton's method. Newton's method is implemented in SageMath™ using the approximations in (10a) and (11a) as the initial starting values. The approximations given in (9a) and (9b) are then used to approximate the derivative function with respect to order. The exact values for ν_j and ν_j' are finally used in the Watson transform formulations defined in (7a) and (7b).

IV. VALIDATION

The results in Section III were validated using simulations from CST [15]. The cylinder and line sources are approximated as a 3D dielectric ellipsoid ($\varepsilon_r = 40$, $\sigma = 2$ *S/m*) and dipole of length 10 cm and loop of radius 0.5 mm for exciting the TE and TM polarizations. The ellipsoid major axis is 1.2 m and the minor axis is 32 cm. The simulated attenuation levels normalized to the $\phi = 0$ and $\rho = 18$ *cm* value vs. ϕ-angle from CST and using the above method are shown in Table 1 for at $\rho' = 17$ *cm*, $\phi' = 0$ and f = 3 GHz. For both polarizations, the results agree to within 8 dB.

Table 1: Attenuation Watson transform (WT) vs. CST

Phi Angle	TE-WT	TE-CST	TM-WT	TM-CST
45 deg	-31.7 dB	-30 dB	-12.7 dB	-18.1 dB
90 deg	-54.6 dB	-54 dB	-24.3 dB	-32.1 dB
135 deg	-76.8 dB	-78.5 dB	-35.7 dB	-44.1 dB
180 deg	-94.1 dB	-93 dB	-41.6 dB	-49.8 dB

V. RESULTS

To illustrate the results from Sections II and III, an example is given. Here, a dielectric cylinder with radius $a = 16$ *cm* assuming the dielectric properties of wet skin are used to approximately model the human torso. Cases are considered for the source located adjacent to the body typical for a WBAN with $\rho' = 17$ *cm*, and $\phi' = 0$.

Figures 2 (a) and 2 (b) show the attenuation levels exterior to the cylinder normalized to the value at the receiver location *for* $\rho = 18$ *cm* vs. ϕ-angle for several frequencies using (4a) and (4b). For the TE polarization, the attenuation is greater than for the TM polarization at each frequency. For both polarizations and for ϕ ~ 180 degrees diffraction effects are apparent in the magnitude responses. These are due to interference caused by clockwise and counterclockwise propagating waves discussed in the next section.

Figures 3 (a) and 3 (b) show the attenuation levels interior to the cylinder normalized to the value at the surface vs. radius (ρ) at 3 GHz for several ϕ-angles using (5a) and (5b). Above this frequency, the attenuation starts to become prohibitively large where the attenuation of the fields interior to the cylinder < 90 dB than those at the surface for both polarizations.

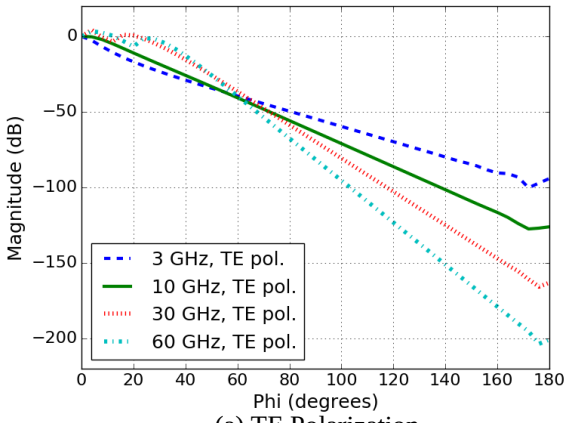

(a) TE Polarization

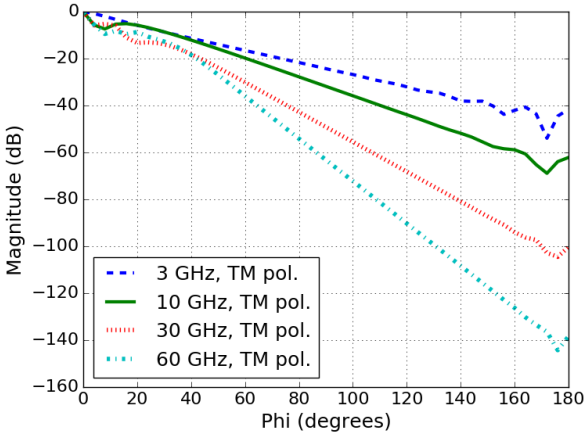

(b) TM Polarization

Fig. 2. Attenuation vs. ϕ-angle and for 3-60 GHz.

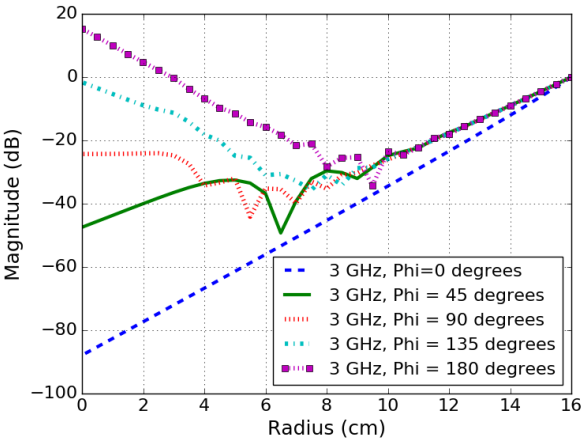

(a) TE polarization

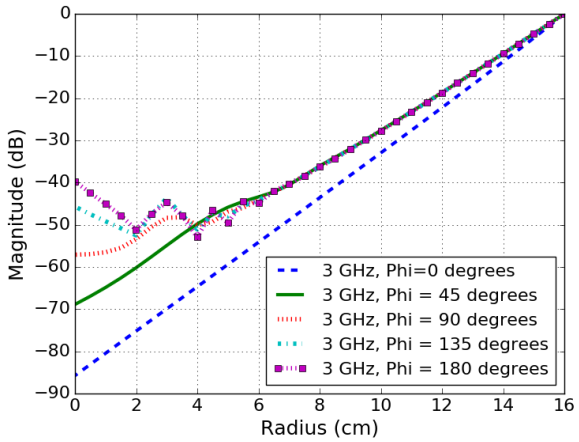

(b) TM polarization

Fig. 3. Attenuation vs. radius (ρ) for fields internal to dielectric cylinder 3 GHz for several ϕ-angle.

Table 2 shows the attenuation level at the center of the dielectric cylinder ($\rho = 0$) normalized to the level at the surface ($\phi = 0$ and $\rho = 16$ *cm*) for some frequencies reserved for biomedical telemetry and ISM applications [16]. Due to limited receiver sensitivity (> -130 dBm) and lower available power levels, the attenuation at the ISM frequencies up to 2.45 GHz is low enough to easily facilitate communications with implanted sensors. At 5.8 GHz, however, the attenuation level is nearly 176 dB for both polarizations.

Table 2: Attenuation levels interior to body for ρ = 0

Frequency	TE (dB)	TM (dB)
195 MHz	-25.8	-18.6
434 MHz	-33.2	-27.1
640 MHz	-36.9	-31.3
915 MHz	-41.2	-36.4
2.45 GHz	-67.9	-65.3
5.8 GHz	-177.2	-176.3

VI. DISCUSSION

Computational issues such as convergence, CPU time, and programming issues are considered. Because SageMath is interpreted, functions such as *fast_callable* and *fast_form* are available to speed-up computation.

A. Series convergence

The residue series solutions for the TE and TM polarizations in (7a) and (7b) both include the term $\frac{\cos \nu (\phi - \pi)}{\sin (\nu \pi)}$, which can be further expanded as:

$$\frac{\cos \nu (\phi - \pi)}{\sin (\nu \pi)} = -i \frac{\exp[i \nu \phi] + \exp[i \nu (2\pi - \varphi)]}{1 - \exp(i \nu 2\pi)}, \quad (12)$$

and can be interpreted as "creeping waves" propagating around the cylinder in the clockwise and counter-clockwise directions. Shown in Figs. 4 and 5 are the magnitudes of (12) for j = 1 to 5 (in ν_j and ν_j') versus angle, ϕ for the previous case with radius, $a = 16$ *cm* and source radius, $\rho' = 17$ *cm* and the dielectric properties for skin for 3 and 30 GHz. These parameters are assumed to be typical for body tissue. For 3 GHz, $n = 6.4 + i\,0.94$, $k_0 a = 10.1$, and $|ka| = 65$. The j = 5 term ($\nu = \nu_5$) magnitude is about 0.01 times the j = 1 ($\nu = \nu_1$) term for $\phi = 28$ *degrees* for the TE and TM cases. For 30 GHz, the j = 5 term ($\nu = \nu_5$) magnitude is about 0.01 times the j = 1 ($\nu = \nu_1$) term for ϕ = 15 degrees for TE case and $\phi = 12$ *degrees* for TM case.

It is clear from the above that the Watson series in (7a) and (7b) converge rapidly for large $k_0 a$ and angle ϕ in the shadow region of the cylinder. For ϕ > 30 degrees, less than five (5) terms are required for convergence for $f \geq 3$ GHz.

B. Use of *fast_callable* SageMath function

The SageMath™ *fast_callable* function transforms algebraic expressions into a form that can be evaluated

quickly. It is especially helpful for expressions that need to be evaluated many times.

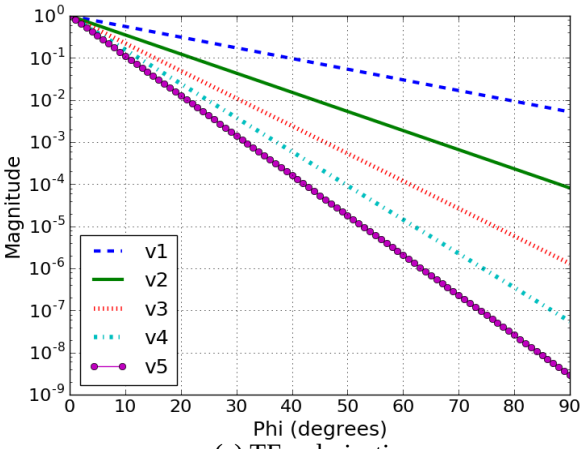

(a) TE polarization

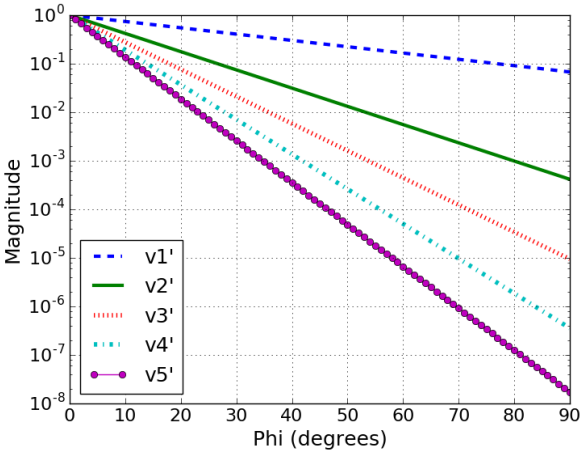

(b) TM polarization

Fig. 4. Convergence (3 GHz).

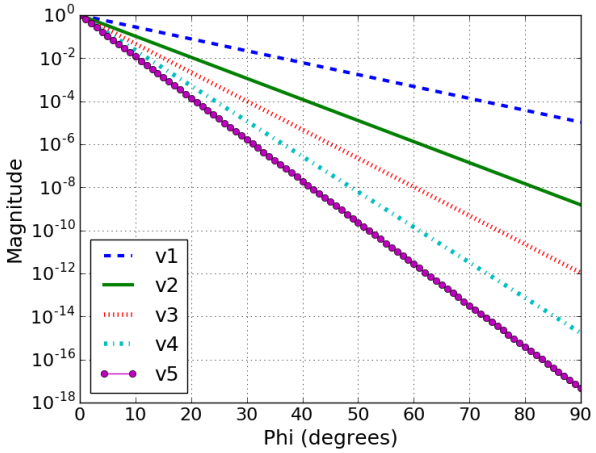

(a) TE polarization

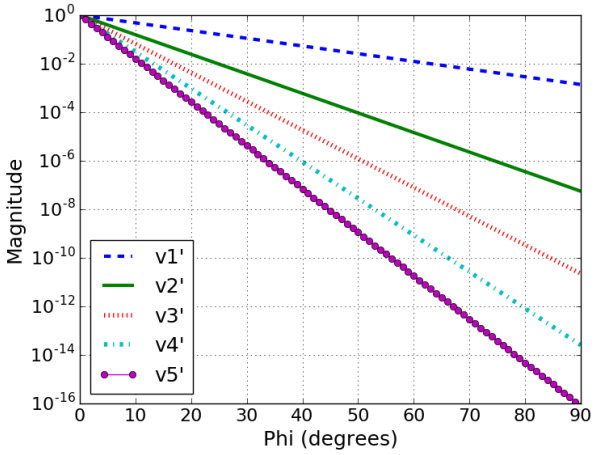

(b) TM polarization

Fig. 5. Convergence (30 GHz).

The Watson transform and the *fast-callable* function were used in calculating the fields for TE and TM polarizations. The timing results are shown below in Table 3 running SageMath^{TM} 6.9 on a Windows 8 PC with an Intel i7-377c 3.4 GHz CPU. The CPU time is reduced by more half by using *fast_callable* with Eqs. (4a) and (4b). Using the Watson transform reduces the CPU time again by nearly a factor of four. Combining the *fast_callable* function with the Watson Transform in Eqs. (7a) and (7b) reduces the CPU time by a factor of at least 77.

Table 3: Timing data for TE and TM cases

Calculation	CPU Time	Speedup
Basic Series (TE)	881.37 sec	----
Basic Series with fast_callable (TE)	369.75 sec	238%
Watson Transform (TE)	94.65 sec	931%
Watson Transform with fast_callable (TE)	11.34 sec	7772%
Basic Series (TM)	885.10 sec	----
Basic Series with fast_callable (TM)	369.05 sec	240%
Watson Transform (TM)	91.90 sec	963%
Watson Transform with fast_callable (TM)	11.09 sec	7981%

VII. CONCLUSION

In this paper, equations for computing the E_z and H_z electromagnetic fields from a lossy dielectric cylinder due to a line source are given. This analysis is

useful for quickly simulating the field penetration into and propagation around the human torso. The Watson transform and fast functions available in SageMath™ are used to significantly speed-up the computation time.

The results from the simulations show that use of frequencies less than 3 GHz result in attenuation levels that are low enough to implement buried implants. The TM polarization is also preferable over TE polarization due to lower propagation attenuation around the torso. This suggests that a preferable radiator could be a small loop or slot antenna with its axis aligned parallel to the body for WBAN applications.

ACKNOWLEDGMENT

The author wishes to thank Dr. Linus Lau of RF Station for CST simulations of the dielectric ellipsoid.

REFERENCES

[1] I. Khan, P. S. Hall, A. A. Serra, A. R. Guraliuc, and P. Nepa, "Diversity performance analysis for on-body communications channels at 2.45 GHz," *IEEE Trans. Antennas Propag*., vol. 57, pp. 956-963, April 2009.

[2] Q. B. Abbasi, M. M. Khan, and Y. Hao, "Diversity antenna techniques for enhanced ultra wideband body-centric communications," *2011 IEEE APSURSI Symp*., pp. 1323-1326, 2011.

[3] T. Mavridis, L. Petrillo, J. Sarrazin, D. Lautru, A. B. Delai, and P. De Doncker, "Creeping wave model of diffraction of an obliquely incident plane wave by a circular cylinder at 60 GHz," *IEEE Trans. Antennas Propag*., vol. 62, no. 3, pp. 1372-1377, March 2014.

[4] L. Petrillo, T. Mavridis, J. Sarrazin, D. Lautru, A. B. Delai, and P. De Doncker, "Analyical creeping wave model and measurements for 60 GHz body area networks," *IEEE Trans. Antennas Propag*., vol. 62, no. 8, pp. 4352-4356, August 2014.

[5] N. Rezaei, D. Majumdar, B. Cockburn, and C. Schlegal, "Electromagnetic energy and data transfer in biological tissues using loop antennas," *2013 International Workshop on Body Area Sensor Networks (BASNet-2013)*, pp. 908-913, 2013.

[6] Sage Math, http://www.sagemath.org/

[7] Dielectric properties of Body Tissues, http:// niremf.ifac.cnr.it/tissprop/htmlclie/htmlclie.php

[8] G. Tyras, *Radiation and Propagation of Electromagnetic Waves*. Academic Press, 1969.

[9] D. S. Jones, *Methods in Electromagnetic Wave Propagation*. 2nd ed., IEEE Press, pp. 522-530, 1995.

[10] Morse and Feshbach, *Methods of Theoretical Physics*. vol. 1, McGraw-Hill, pp. 467, 817, 1953.

[11] NIST Handbook of Mathematical Functions, Cambridge University Press, p. 227, 2010.

[12] Y. A. Brychkov, "Higher derivatives of the Bessel functions with respect to the order," *Integral Transforms and Special Functions*, April 2016.

[13] S. E. Sandstrom and C. Ackren, "Note on the complex zero's of $H'_\nu(x) + i\zeta H_\nu(x) = 0$," *Journal of Computational and Applied Mathematics*, 201, pp. 3-7, 2007.

[14] J. O. Cochran, "The zeroes of Hankel functions as functions of their order," *Numerische Mathematik*, 7, pp. 238-250, 1965.

[15] CST Microwave Studio, Darmstadt, Germany.

[16] Title 47, CFR Part 15 - Radio Frequency Devices, US Government Printing Office, 2015.

Grant Andrew Ellis received the Ph.D. degree in Electrical Engineering from the University of Washington, Seattle, in 1995. He has more than 25 years of professional experience in the areas of RF and Microwave and antenna analysis and design. Ellis has written over 40 papers and publications and holds 5 US patents. Ellis is the Founding Chairman of the IEEE MTT/ED/AP Penang Chapter. He is a registered professional engineer, a Member of ACES, and has been a Senior Member of the IEEE since 2004.